
Preflight Transient Dynamic Analyses of B-52 Aircraft Carrying Space Shuttle Solid Rocket Booster Drop-Test Vehicle

William L. Ko and Lawrence S. Schuster

January 1984

LIBRARY COPY

JAN 30 1984

LANGLEY RESEARCH CENTER
LIBRARY, NASA
HAMPTON, VIRGINIA



National Aeronautics and
Space Administration

9 54 54 AU/KO, W. L.
10 4 4 AU/SCHUSTER, L. S.

DISPLAY 10/2/3

84N15588*# ISSUE 6 PAGE 858 CATEGORY 39 RPT#: NASA-TM-84925 H-1197

NAS 1.15:84925 84/01/00 17 PAGES UNCLASSIFIED DOCUMENT

Previously announced as A84-13725

UTTL: Preflight transient dynamic analyses of B-52 aircraft carrying Space Shuttle solid rocket booster drop-test vehicle TLSP: Final Report

AUTH: A/KO, W. L.; B/SCHUSTER, L. S.

CORP: National Aeronautics and Space Administration. Ames Research Center, Moffett Field, Calif. AVAIL. NTIS SAP: HC A02/MF A01

Presented at the AIAA 2nd Flight Test Conf., Las Vegas, Nev., 16-18 Nov. 1983

MAJS: /*B-52 AIRCRAFT/*DYNAMIC STRUCTURAL ANALYSIS/*LANDING GEAR/*PREFLIGHT

■

Preflight Transient Dynamic Analyses of B-52 Aircraft Carrying Space Shuttle Solid Rocket Booster Drop-Test Vehicle

William L. Ko and Lawrence S. Schuster

NASA Ames Research Center, Dryden Flight Research Facility, Edwards, California 93523

1984



National Aeronautics and
Space Administration

Ames Research Center

Dryden Flight Research Facility
Edwards, California 93523

N84-15588[#]

PREFLIGHT TRANSIENT DYNAMIC ANALYSES OF B-52 AIRCRAFT CARRYING
SPACE SHUTTLE SOLID ROCKET BOOSTER DROP-TEST VEHICLE

William L. Ko* and Lawrence S. Schuster*
NASA Ames Research Center, Dryden Flight Research Facility
Edwards, California

Abstract

This paper concerns the transient dynamic analysis of the B-52 aircraft carrying the Space Shuttle solid-rocket booster drop-test vehicle (SRB/DTV). The NASA structural analysis (NASTRAN) finite-element computer program was used in the analysis. The B-52 operating conditions considered for analysis were 1) landing and 2) braking on aborted takeoff runs. The transient loads for the B-52 pylon front and rear hooks were calculated. The results can be used to establish the safe maneuver envelopes for the B-52 carrying the SRB/DTV in landings and brakings.

Nomenclature

A	= dynamic-load scale factor	K_Y	= spring constant for pylon yaw motion, in.·lb
D_{CL}	= left-rear-hook drag load, lb	[M]	= mass matrix
E	= Young's modulus of bar element, lb/in. ²	M_6	= braking moment at grid point 6, lb·in.
F	= dynamic load, lb	M_{15}	= braking moment at grid point 15, lb·in.
F_6	= front landing gear braking force at grid point 6, lb	m	= mass of DTV, lb·sec ² /in.
F_{15}	= rear landing gear braking force at grid point 15, lb	P_6	= front landing gear reaction force, lb
G	= shear modulus of bar element, lb/in. ²	P_{15}	= rear landing gear reaction force, lb
g	= gravitational acceleration, 386.4 in./sec ²	S_A	= front-hook side load, lb
h_6	= front landing gear length, in.	S_{CL}	= rear-hook side load, lb
h_{15}	= rear landing gear length, in.	t	= time, sec
I_{ij} (i, j = 1, 2, 3)	= moments of inertia of nodal weight based on $[x_1, x_2, x_3]$ system, lb·in. ²	V_A	= front-hook total vertical load, lb
I_P (or I_Y)	= pitching (or yawing) moment of inertia of DTV, lb·in. ²	V_{AD}	= front-hook dynamic vertical load, lb
I_R	= rolling moment of inertia of DTV, lb·in. ²	V_{AS}	= front-hook static vertical load, lb
K_P	= spring constant for pylon pitching motion, in.·lb	V_{CL}	= left-rear-hook dynamic vertical load, lb
K_S	= spring constant for pylon side motion, lb/in.	V_{CLD}	= left-rear-hook dynamic vertical load, lb
		V_{CLS}	= left-rear-hook static vertical load, lb
		V_S	= sink velocity of B-52, ft/sec
		W	= weight of mass element (nodal weight), lb
		W_{B52}	= weight of B-52, lb
		W_{DTV}	= DTV weight, lb
		W_6	= weight on front landing gear, lb
		W_{15}	= weight on rear landing gear, lb
		x, y, z	= global rectangular Cartesian coordinates used in NASTRAN model, in.
		x_1, x_2, x_3	= local rectangular Cartesian coordinates for mass element used in NASTRAN model, in.

*Aerospace Engineer. Member AIAA.

This paper is declared a work of the U.S. Government and therefore is in the public domain.

θ	= B-52 nose-up angle, deg
$\theta_x, \theta_y, \theta_z$	= rotation about the x-, y-, or z-axis, rad
μ	= coefficient of friction between landing gear tires and the ground surface
τ	= delay time, sec
τ_0	= braking force ramp rise time, sec
ω_p	= vibration frequencies of pylon in pitching motion, 1/sec
ω_s	= vibration frequencies of pylon in side motion, 1/sec
ω_y	= vibration frequencies of pylon in yaw motion, 1/sec
$[\dot{\quad}], [\ddot{\quad}]$	= time derivatives, 1/sec, 1/sec ²

Introduction

The performance of the decelerator system (i.e., the main parachute) of the Space Shuttle solid-rocket booster (SRB) was investigated by using a scale model drop-test vehicle (DTV). The DTV, which carried only one main parachute (the actual SRB has three main parachutes), was attached to a pylon on the NASA B-52 carrier aircraft by means of one front hook and two rear hooks (see Figs. 1 and 2). The DTV was then carried to high altitude and released from the B-52 to test the deployed SRB main parachute.

In the past captive flights (i.e., no releasing of the DTV from the B-52), the B-52 pylon front hook was loaded up to considerable levels. The most serious instances were the quarter-elevator throws (the front hook load reached 89% of the limit load of 37,700 lb), ground turns (the front hook load reached 79% of the limit load), and landings (the front-hook load reached 76% of the limit load). Because of these recorded high loading levels of the front hook, there is concern about possible overloadings of the front hook in an upcoming new series of DTV tests.

In order to reduce the pitching moment of inertia and thereby reduce the front-hook dynamic loadings, the DTV was shortened slightly. Before testing the revised DTV system, it was necessary to perform preflight transient dynamic analyses of the entire B-52/DTV system, and to estimate the range of the front-hook loadings under conditions imposed by various maneuvers of the B-52. This paper concerns the transient dynamic analysis of the B-52/DTV system when either landing or braking on aborted takeoff runs. The front- and the rear-hook loading levels calculated under different landing and braking conditions can then be used to establish the safe maneuver envelopes for the B-52 carrier aircraft.

Transient Dynamic Analyses

NASTRAN Finite-Element Modeling

The NASA Structural Analysis (NASTRAN) finite-element computer program¹ was used in the transient dynamic analysis of the B-52/DTV system. As shown in Fig. 2, the B-52 carrier structure was modeled by using CBAR elements (uniform cross section bar element) for carrying the structural stiffnesses; the B-52 structural masses were lumped at most of the grid points, and were modeled by using C0NML elements (concentrated mass elements of type 1) for carrying the structural inertia effect. Landing gears were not modeled. Grid points 9, 17, 26, 43, 62, 64, 71, and 73 are massless points; therefore, they were removed in the dynamic analyses with OMIT cards. Figure 3 shows the NASTRAN model of the B-52 carrying the DTV. The front and rear landing gears are located at grid points 6 and 15, respectively. The center of gravity of the B-52 varies between grid points 12 and 13. Because of very high stiffnesses, elements lying between grid-points 7 and 9, 9 and 10, 16 and 17, 23 and 26, and 24 and 43, were modeled as rigid elements, using CRIGD1 constraints (rigid constraints of type 1).

The vertical tail has extremely high vertical bending stiffness (about the y-axis); therefore, CRIGD2 constraints (rigid constraints of type 2) were used to force the entire vertical tail to rotate as a whole about the y-axis. Namely, rotations about the y-axis of grid-points 27 through 35 were made identical to those of grid-point 26. Also, because of very high lateral bending stiffness (about z) of the wing roots, rotations about the z-axis of grid-points 67 and 68 were set equal to that of grid-point 9 through the use of CRIGD2 constraints. The reason for using the above rigid constraints CRIGD1 and CRIGD2 was to avoid the solution errors caused by using very large values of stiffnesses for the CBAR elements.

For each C0NML element, a local rectangular Cartesian coordinate system (x_1, x_2, x_3) (with origin located at the associated mass grid point) was defined by using C0RD2R cards. At each mass grid point, the mass matrix $[M]$ was set up in the (x_1, x_2, x_3) system for input to the C0NML card. Because the centers of mass of most of the C0NML elements were offset from the associated grid points, some of the off-diagonal terms in $[M]$ shown below were nonzero:

$$[M] = \frac{1}{g} \begin{bmatrix} W & 0 & 0 & 0 & x_3W & -x_2W \\ & W & 0 & -x_3W & 0 & x_1W \\ & & W & x_2W & -x_1W & 0 \\ & & & I_{11} & -I_{12} & -I_{13} \\ \text{[symmetry]} & & & & I_{22} & -I_{23} \\ & & & & & I_{33} \end{bmatrix} \quad (1)$$

where W is the weight of the C0NML element (or C0NML2 element described below), and I_{ij} ($i, j = 1, 2, 3$) are the weight moments of inertia of the C0NML element (or C0NML2 element) referred to the (x_1, x_2, x_3) system. The DTV was modeled by using one C0NML2 element (concentrated mass element of type 2) with the DTV center of mass

located at grid point 85 (no mass offset). The mass matrix [Eq. (1)] of this CØNM2 element is based on a local rectangular Cartesian coordinate system, with the origin at grid-point 85, defined by using a CØRD2R card. The mass of the pylon was lumped at grid-point 70 and was represented by a CØNM1 element whose mass matrix [Eq. (1)] is based on a local rectangular Cartesian coordinate system, with origin at grid-point 70, defined by a CØRD2R card. In the data input to the mass matrix [Eq. (1)] for all the mass elements CØNM1 and CØNM2, weight was used, which was converted into mass through the use of a PARAM/WTMASS card.

In modeling the pylon, two cases were considered: a rigid pylon and an elastic pylon. For the case of the rigid pylon, grid-point 85 was rigidly attached to grid-point 70 through a CRIGD1 rigid constraint. For the elastic pylon, a CRIGD2 card was used to rigidly couple the motions in the x- and z-directions of grid-point 85 to those of grid-point 70 (i.e., perfectly rigid in z-extension, infinite shear stiffness in the x-z plane). The rest of the degrees of freedom were set free (see Fig. 4). For the yaw motion, a torsional spring CELAS2 element was attached between grid-points 70 and 85 (Fig. 4a) to allow spring resistance only in yaw motion (sixth degree of freedom). For the roll motion (or side motion), a CRIGD1 rigid element was attached between grid-points 70 and 87 (grid-point 87 is coincidental with grid-point 85). A spring CELAS2 element was then attached between grid-points 85 and 87, permitting the motion of grid-point 85 only in y-direction (second degree of freedom) (Fig. 4b). Lastly, the pitching elastic resistance was modeled by connecting a bending spring element CELAS2 between grid-points 70 and 85, permitting only the pitching motion (fifth degree of freedom) of the pylon (Fig. 4c). The spring constants for the above three CELAS2 elements were calculated from the measured vibration frequencies (derived from X-15 reports) using the following equations:

$$K_Y = \frac{I_Y \omega_Y^2}{g} ; \quad I_Y \approx I_P \quad (2)$$

$$K_S = m \omega_S^2 \quad (3)$$

$$K_P = \frac{I_P \omega_P^2}{g} \quad (4)$$

where K_Y , K_S , and K_P are, respectively, spring constants for yaw, side, and pitching motions; m is the mass of the DTV; I_P and I_Y are, respectively, the pitching and the yawing moments of inertia of DTV; and ω_Y , ω_S , and ω_P are, respectively, angular vibration frequencies in yaw, side, and pitching motions.

The entire B-52/DTV NASTRAN model has 88 grid points, 78 CBAR elements, 7 CRIGD1 elements, 76 CØNM1 elements, and 1 CØNM2 element. The NASTRAN model free system is supported at grid-points 12 (with components, 1, 2, 3, and 4 constrained) and 13 (with components 2 and 3 constrained) through the use of a SUPORT card which is to remove the stress-free, rigid-body motion component from the free system.

Forcing Functions

In the landing analyses, four cases of landing conditions were considered, and are shown below:

Case	Sink speed V_S , ft/sec	Nose-up angle, deg	Front landing gear touchdown delay time τ , sec
1	3	3	0.82
2	3	6	1.30
3	3	0	0.
4	6	3	0.47

The landing-gear reaction forces (obtained from the manufacturer) at the fuselage for the case $V_S = 3$ ft/sec, $\theta = 3^\circ$, are shown in Figs. 5 and 6. The landing-gear reaction forces for the remaining three cases are similar and, therefore, are not shown. Those landing forces are to be applied at grid-points 6 (front-landing-gear attach point) and 15 (rear-landing-gear attach point) of the NASTRAN model. Those forcing functions (e.g., Figs. 5 and 6) were converted into tables by using TABLED1 cards for input to the NASTRAN model. The TABLED1 cards were used in conjunction with the following cards in the Bulk Data Deck:

TLØAD1 = Define a time-dependent dynamic load of the form $AF(t - \tau)$

DAREA = Define the dynamic load scale factor A

DELAY = Define the dynamic load delay time τ

DLØAD = Combination of dynamic load

Also, in the Case Control Deck, the dynamic load set must be defined through $DLØAD = n$, where n is the set identification number. The initial velocity (sink velocity, in the negative z-direction) of the NASTRAN model was defined by using TIC cards in the Bulk Data Deck for all the grid points excluding the massless grid points and the rigid element grid points. In the Case Control Deck, the transient initial condition set must be selected through the use of $IC = n'$ where n' is the set identification number. The integration time-steps and the solution output time-intervals were specified by using a TSTEP card in the Bulk Data Deck. The time-delay effect (τ) of the front-landing-gear forcing function can be handled in two ways:

1) Without using the DELAY card, construct the front-landing-gear forcing function table TABLED1 in such a way that the delay time is absorbed into the table

2) Using the DELAY card, construct the front-landing-gear forcing function table TABLED1 by shifting the time origin to the force rising time [i.e., by using $(t - \tau)$ as the time scale]

In the braking analyses, the transient dynamic forcing functions (landing-gear braking force or braking moment) for input to the NASTRAN model are shown in Fig. 7. The coefficient of friction μ between the landing-gear tires and the ground

surface was taken to be 0.55. Brakes were applied when the B-52 was taxiing at 135 knots (2734.25 in./sec). The lengths of braking force ramp-rise-time τ_0 (Fig. 7) considered in the braking analyses are

Case	τ_0 , sec
1	0.2
2	0.5
3	1.0

The braking forces and the associated braking moments at the landing-gear attach points 6 and 15 are given by

$$F_6 = \mu W_6 \quad (5)$$

$$F_{15} = \mu W_{15} \quad (6)$$

$$M_6 = h_6 F_6 \quad (7)$$

$$M_{15} = h_{15} F_{15} \quad (8)$$

where W_i ($i = 6, 15$) is the weight on the landing gear at grid-point i , where F_i ($i = 6, 15$) and M_i ($i = 6, 15$) are, respectively, the braking force and the braking moment at grid-point i , and where h_i ($i = 6, 15$) is the length of the landing gear. The braking forcing functions and the initial conditions were input into the NASTRAN model in a way similar to that used in the landing analyses. DELAY cards may be omitted since there is no time delay of the front-landing-gear forcing function.

Input Data for Structural Model

The grid-point coordinates, nodal weight, and stiffness data for input to the B-52 NASTRAN model and the inertia data for input to Eq. (1) were taken from Ref. 2. Other input data are

$$E = 10 \times 10^6 \text{ lb/in.}^2$$

$$G = 4 \times 10^6 \text{ lb/in.}^2$$

$$\text{B-52 structural damping coefficient} \\ = 0.015 \text{ lb}\cdot\text{sec/in.}$$

$$\text{DTV weight } W_{DTV} = mg = 49,000 \text{ lb}$$

$$\text{DTV pitching (or yawing) moment of inertia} \\ I_p = 1.4591 \times 10^9 \text{ lb}\cdot\text{in.}^2$$

$$\text{DTV rolling moment of inertia} \\ I_R = 4.5537 \times 10^7 \text{ lb}\cdot\text{in.}^2$$

$$\text{Pylon weight} = 1170 \text{ lb}$$

Pylon mass matrix:

$$[M]_{\text{pylon}} = \frac{1}{g} \begin{bmatrix} 1170. & 0. & 0. & 0. & -22670. & 0. \\ & 1170. & 0. & 22670. & 0. & -32683. \\ & & 1170. & 0. & 32683. & 0. \\ & & & 3.6949 \times 10^6 & 0. & 0. \\ & & & & 3.0268 \times 10^6 & 0. \\ & & & & & 1.1423 \times 10^6 \end{bmatrix} \quad (9)$$

[symmetry]

The pylon mass matrix is based on the pylon mass local rectangular Cartesian coordinate system $[x_1, x_2, x_3]$ with origin at grid-point 70, as shown in Fig. 2. Pylon vibration frequencies are as follows:

$$\omega_Y = 13.42 \text{ 1/sec}$$

$$\omega_S = 15.01 \text{ 1/sec}$$

$$\omega_P = 16.49 \text{ 1/sec}$$

Pylon spring constants:

$$K_Y = 6.7970 \times 10^8 \text{ in.}\cdot\text{lb}$$

$$K_S = 2.8583 \times 10^4 \text{ lb/in}$$

$$K_P = 1.0267 \times 10^9 \text{ in.}\cdot\text{lb}$$

Results

Figures 8 and 9, respectively, show the responses of the B-52 NASTRAN model at $t = 1.0$ sec and $t = 2.1$ sec, subjected to an upward (+z-direction) triangular force pulse (fictitious landing-gear forces) of 1.5-g magnitude applied at the front and rear landing gears. For this sample case, SPC constraints were applied at grid-points 12 (components 1, 2, 3, and 4 constrained) and 13 (components 2 and 3 constrained). Notice that the two outboard engines are under considerable pitching motions at $t = 2.1$ sec (Fig. 9). Figures 10 and 11, respectively, show the acceleration in the z-direction (\ddot{z}) and the angular acceleration ($\ddot{\theta}_y$) about the y-axis at grid-point 85 (DTV) for both elastic and rigid pylons for a sink rate $V_S = 3$ ft/sec and a nose-up angle $\theta = 3^\circ$. The \ddot{z} (Fig. 10) for both the elastic and rigid cases are quite close, having about 5 cycles/sec of oscillations. Using the hook-loads equations given in the Appendix, all the time-histories of the hook loads were calculated; they are shown in Figs. 12-16 for $V_S = 3$ ft/sec, $\theta = 3^\circ$, for both the elastic and rigid pylons. The front-hook vertical loads V_A for both the elastic and rigid pylons are quite close (Fig. 12), with the peak value (elastic case) reaching 73% of the limit load of 37,700 lb. The amplitudes of oscillations of the front-hook side load S_A (Fig. 13), the rear-hook vertical load V_{CL} (Fig. 14), and the rear-hook side load S_{CL} (Fig. 15) are less for the elastic case than for the rigid case. However, the reverse is true for the rear-hook drag load D_{CL} (Fig. 16). Notice that the peak value of the front-hook side load S_A for the rigid pylon (Fig. 13) exceeded the limit load, and that the elastic effect greatly reduced the peak value of S_A .

The peak value of V_{CL} reached only 38% of the limit value of 57,600 lb. The time-histories of the hook loads for the rest of the landing conditions - $V_S = 3$ ft/sec, $\theta = 6^\circ$; $V_S = 3$ ft/sec, $\theta = 0^\circ$ (simultaneous touchdown of the front and rear landing gears); and $V_S = 6$ ft/sec, $\theta = 3^\circ$ are quite similar to the case in which $V_S = 3$ ft/sec, $\theta = 3^\circ$; therefore, they are not shown here. The calculated peak values of V_A , V_{CL} , S_A , S_{CL} , and D_{CL} for the elastic pylon for the four landing conditions are listed in Table 1; the peak values of V_A and V_{CL} are plotted in Figs. 17 (V_A) and 18 (V_{CL}). The landing condition ($V_S = 6$ ft/sec, $\theta = 3^\circ$) induced the highest peak values of V_A (86% of limit load) and V_{CL} (48% of limit load). Figures 19 and 20, respectively, show \ddot{z} and $\ddot{\theta}_y$ at grid-point 85 (DTV) for the braking condition at $\tau_0 = 0.2$ sec, $\mu = 0.55$, for both elastic and rigid pylons. The \ddot{z} for the braking is insignificant when compared with $\ddot{\theta}_y$ which has about 3 cycles/sec of oscillation for both elastic and rigid cases.

All the calculated time-histories for the hook loads (see Appendix) are shown in Figs. 21-25 for the braking condition at $\tau_0 = 0.2$ sec, $\mu = 0.55$, for both elastic and rigid pylons. Notice that the rear-hook drag load D_{CL} (Fig. 25) reflects the shape of braking forcing function. The time histories of the hook loads for the other two braking conditions - $\tau_0 = 0.5$ sec, $\mu = 0.55$ and $\tau_0 = 1.0$ sec, $\mu = 0.55$ - are similar to the case $\tau_0 = 0.2$ sec; therefore, they are not shown. The braking tends to decrease the mean value of V_A from its static value and increase the mean value of V_{CL} from its static value. However, the peak values of V_{CL} stay well below the limit value. The peak values of V_A , V_{CL} , S_A , S_{CL} , and D_{CL} for the elastic pylon for the three braking conditions are tabulated in Table 1, and the peak values of V_A , V_{CL} , and D_{CL} are plotted in Figs. 26-28. The braking condition $\tau_0 = 0.2$ sec, $\mu = 0.55$ gives the highest peak values of V_A (39% of the limit load), V_{CL} (46% of the limit load), S_A (89% of the limit load), S_{CL} (41% of the limit load), and D_{CL} (53% of the limit load). The peak values of V_A for all three cases stay close to its static value.

Summary

The NASTRAN finite-element computer program was used in transient dynamic analyses of a B-52 aircraft carrying the Space Shuttle solid-rocket booster drop-test vehicle when either landing or braking. All the hook loads of the B-52 pylon were calculated for different landing and braking conditions. Both elastic and rigid pylons were considered. For landing, it was found that the vertical hook loads were more sensitive to the landing conditions than side and drag loads. The landing condition (6-ft/sec sink rate, 3° nose-up) was found to be the worst case; it caused the peak value of V_A to reach 86% of its limit load, and the peak value of V_{CL} to reach 48% of its limit load. For braking, the peak values of V_A and V_{CL} are relatively insensitive to the braking conditions, but the side loads of both front and rear hooks oscillate considerably about their static values (i.e., zero). The rear-hook drag load was quite sensitive to the braking conditions. Braking tends to decrease the front-hook mean vertical load, and slightly increase the rear-hook

vertical load from their respective static values.

The information on the hook loads can now be used as a basis to establish safe maneuver envelopes for the B-52 carrying the SRB/DTV when landing or braking.

Appendix: Equations for Hook Loads

The following equations for hook loads were developed in accordance with the dimensions shown in Figs. 29 through 31.

1) Front-hook dynamic vertical load V_{AD} (considering moment about point A) (Fig. 30a):

$$V_{AD} = \frac{1}{211.0} \left(m\ddot{z}(60.8) - m\ddot{x}(27.35 - 17.5) + \{I_p + m[(60.8)^2 + (27.35 - 17.5)^2]\}\ddot{\theta}_y \right) \quad (A1)$$

2) Front-hook static vertical load V_{AS} :

$$V_{AS} = \frac{60.8}{211.0} W_{DTV}; \quad W_{DTV} = mg \quad (A2)$$

3) Front-hook total vertical load V_A :

$$V_A = V_{AD} + V_{AS} \quad (A3)$$

4) Front-hook side load S_A (considering equivalent moment about point O) (Fig. 30b):

$$S_A = \frac{1}{220.29} \{ m\ddot{y}(60.8) - [I_p + m(60.8)^2]\ddot{\theta}_z \} \quad (A4)$$

where 220.29 is the equivalent moment arm (from Ref. 3).

5) Rear-hook dynamic vertical load V_{CLD} (considering moment about point CR) (Fig. 31):

$$V_{CLD} = \frac{1}{62.624} \left((m\ddot{z} - V_{AD})(31.312) - m\ddot{y}(9.85) - S_A(16.3125) - \{I_R + m[(9.85)^2 + (31.312)^2]\}\ddot{\theta}_x \right) \quad (A5)$$

6) Rear-hook static vertical load V_{CLS} :

$$V_{CLS} = \frac{1}{2} \frac{150.2}{211.0} W_{DTV} \quad (A6)$$

7) Rear-hook total vertical load V_{CL} :

$$V_{CL} = V_{CLD} + V_{CLS} \quad (A7)$$

8) Rear-hook side load S_{CL} :

$$S_{CL} = m\ddot{y} - S_A \quad (A8)$$

9) Rear-hook drag load D_{CL} (considering equivalent moment about point O) (Fig. 30b):

$$D_{CL} = \frac{1}{1484.475} \{ [I_P + m(60.8)^2] \ddot{\theta}_z - m\ddot{y}(60.8) \} + \frac{1}{2} m\ddot{x} \quad (A9)$$

where 1484.475 is the equivalent moment arm (from Ref. 3).

References

¹"NASTRAN Theoretical Manual, NASTRAN Users' Manual," Computer Software Management and Information Center (COSMIC), Ballows Halls, University of Georgia, Atlanta, Ga., 1978.

²Hull, D. L. and Roger, K. L., "B-52E CCV Flight Test Data Applicable to Parameter Estimation," Air Force Flight Dynamics Laboratory TR-75-131, 1975.

³Quade, D. A., "Load and Dynamic Assessment of B-008 Carrier Aircraft for Configuration 1 and 2 Space Shuttle Solid Rocket Booster Deceleration Subsystem Drop Test Vehicles. Vol. IV, Pylon Load Data Method 2," Contract No. NA58-31805, Boeing Aircraft Company Report D3-11220-1, 1977.

Table 1 Peak hook loads associated with different landing and braking conditions

Condition		V_A , lb (% load limit)	V_{CL} , lb (% load limit)	S_A , lb	S_{CL} , lb	D_{CL} , lb
Landing						
V_S , ft/sec	θ , deg					
3	0	21,870(58%)	20,220(35%)	1,708(20%)	4,457(18%)	4,190(13%)
3	3	27,703(73%)	21,751(38%)	3,206 ^a	5,196(21%)	8,667(28%)
3	6	32,083(85%)	23,371(41%)	3,004 ^a	8,335 ^a	11,733 ^a
6	3	32,600(85%)	27,682(48%)	3,042 ^a	5,637 ^a	9,957 ^a
Braking						
τ_0 , sec						
1.0		14,138(38%)	22,138(38%)	1,513(17%)	1,134(5%)	14,278(46%)
0.5		14,157(38%)	22,895(40%)	2,359(27%)	2,646(11%)	14,643(47%)
0.2		14,888(39%)	26,638(46%)	7,717(89%)	9,984(41%)	16,717(53%)
Limit load, lb						
		37,700	57,600	8,667	24,501	31,290

^aPeak values within $t = 3$ sec limit of computation; actual peak values could be higher.

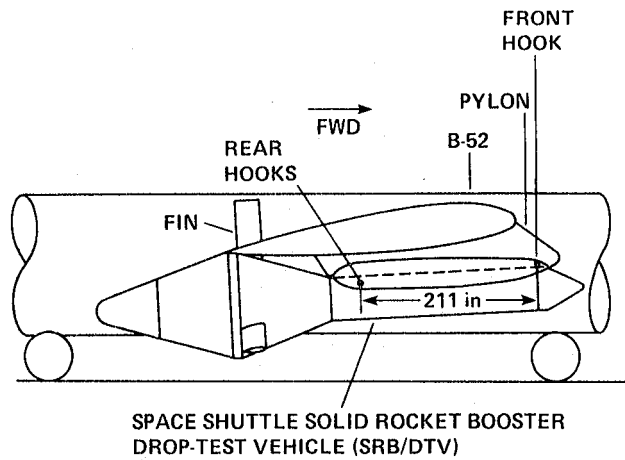


Fig. 1 Geometry of Space Shuttle solid-rocket booster drop-test vehicle (DTV) attached to B-52 pylon; view looking inboard at right side of B-52 and SRB/DTV.

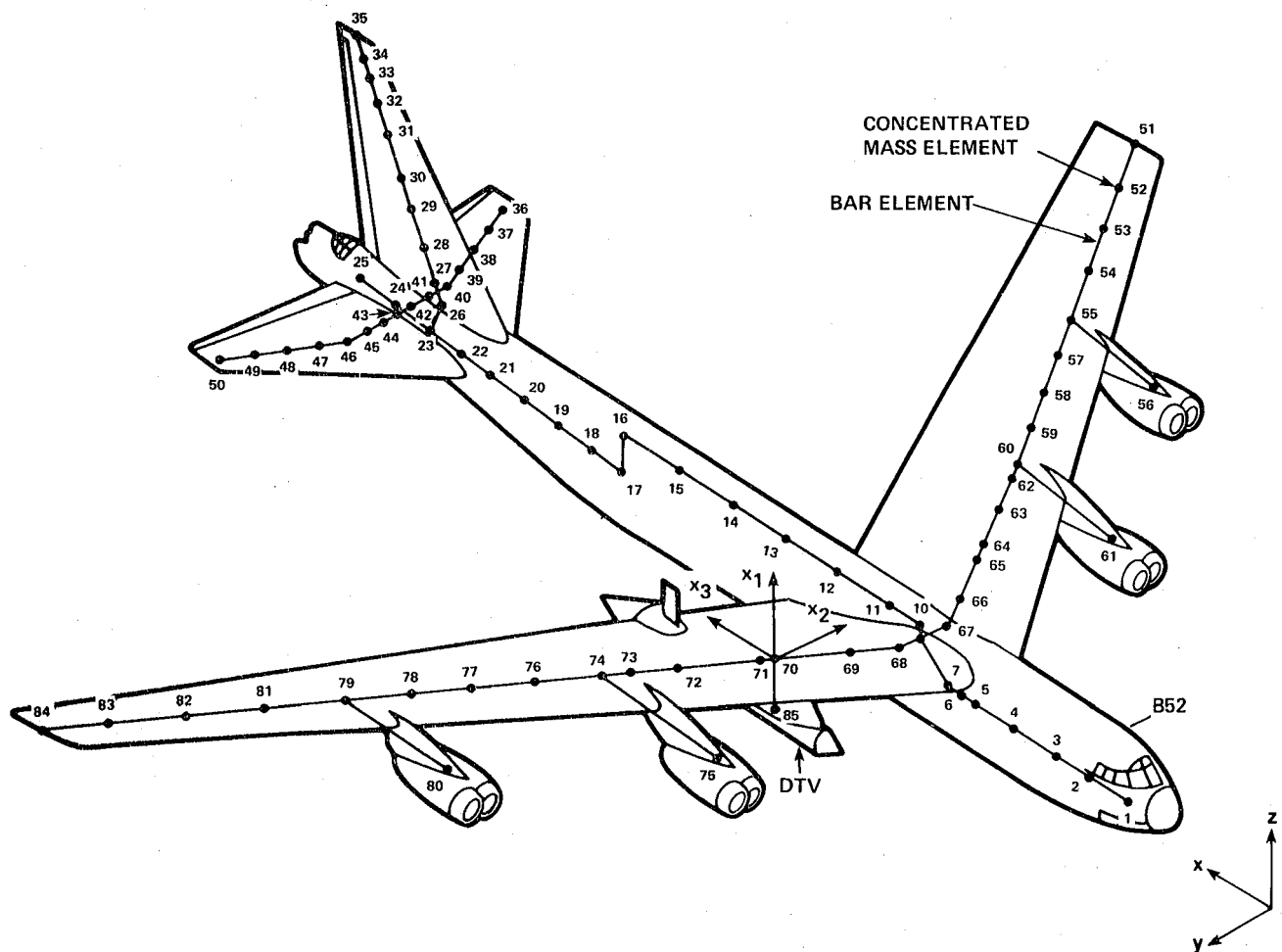


Fig. 2 B-52 structure represented by bar elements and concentrated mass elements.

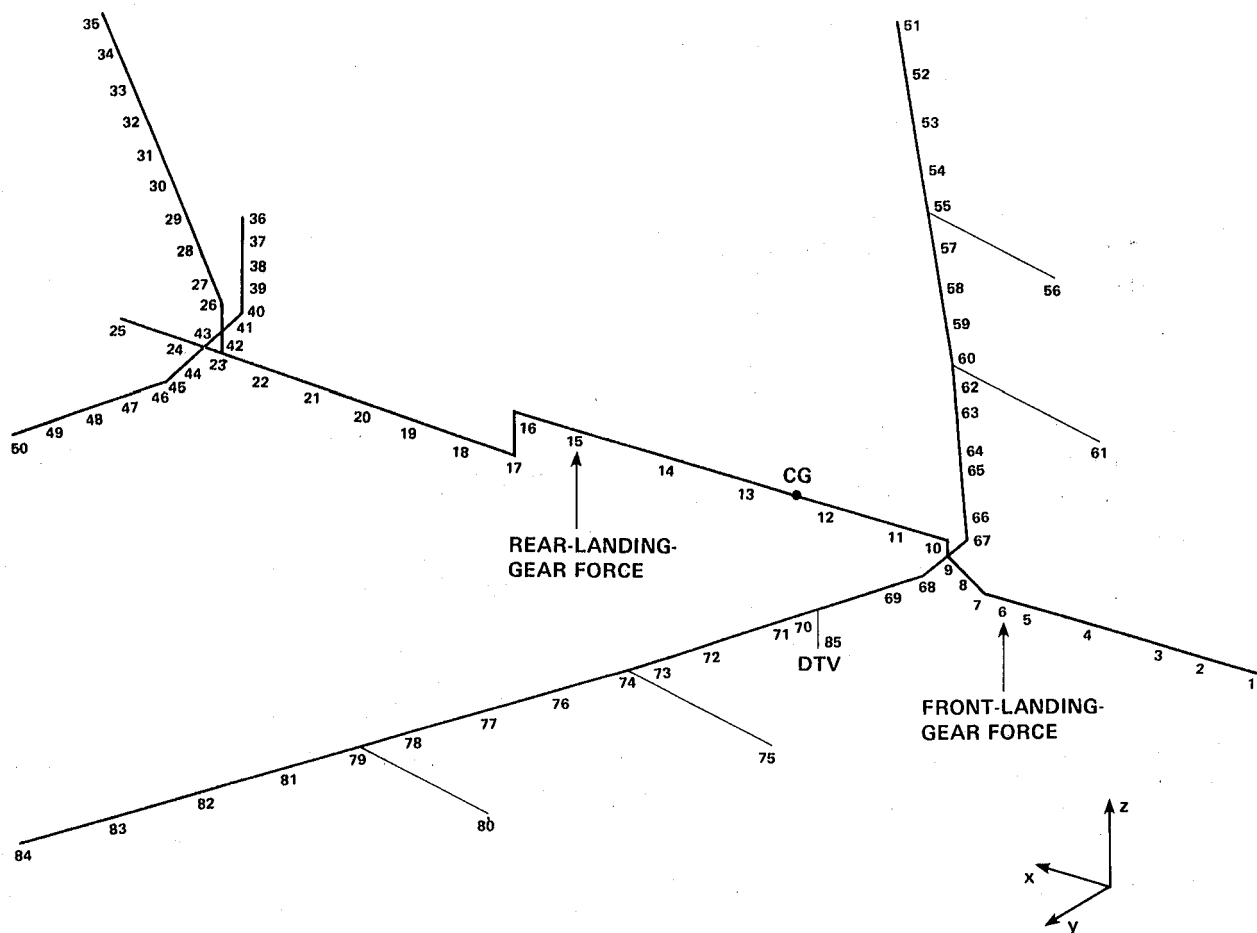


Fig. 3 B-52 NASTRAN model.

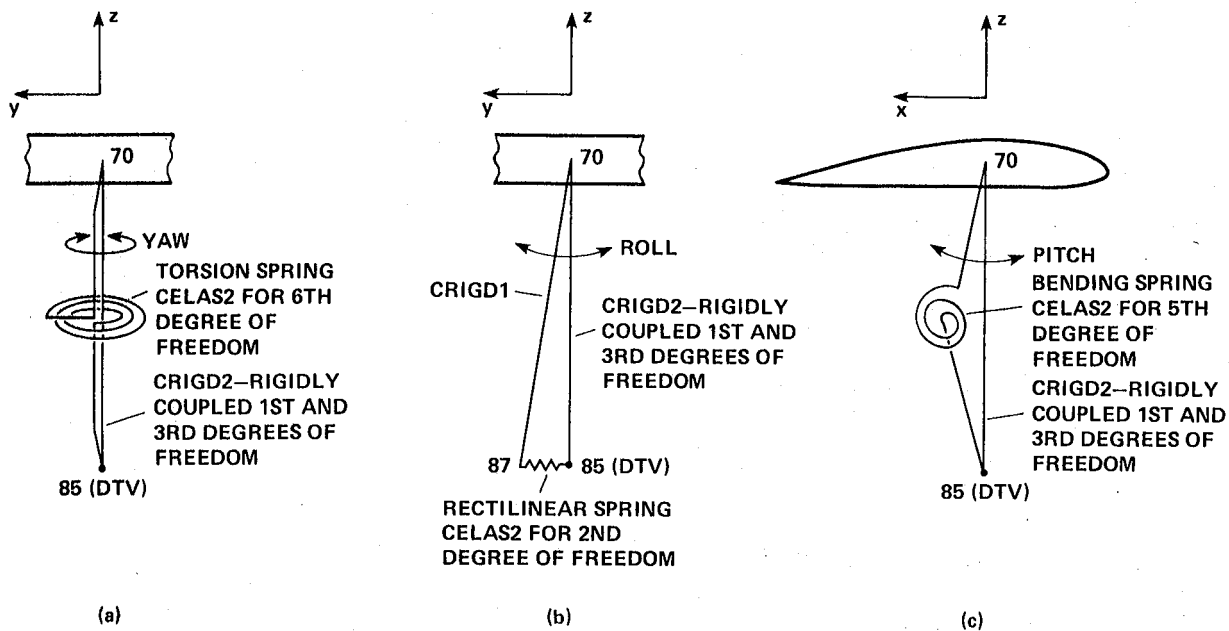


Fig. 4 Modeling of elastic pylon. a) Yaw, b) roll, c) pitch.

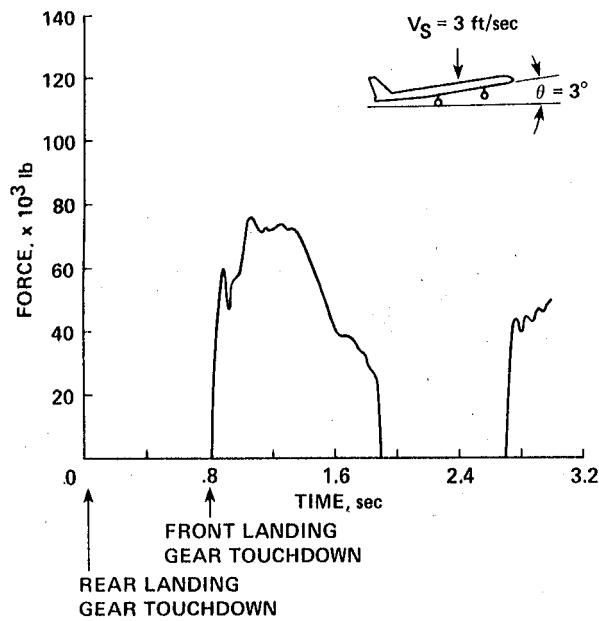


Fig. 5 Combined front landing gear force:
 $V_S = 3$ ft/sec, $\theta = 3^\circ$.

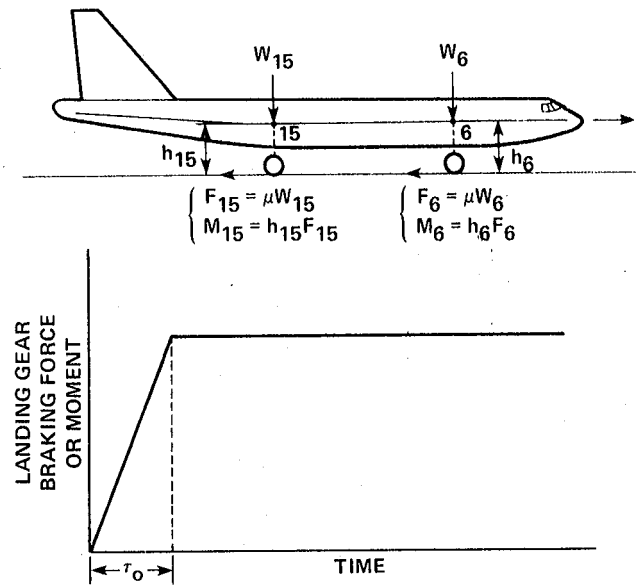


Fig. 7 Landing-gear braking force (or moment) curve.

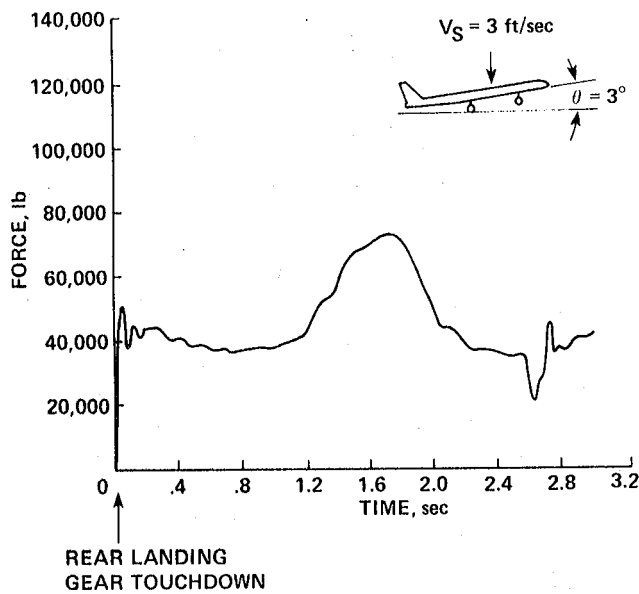


Fig. 6 Combined rear landing gear force:
 $V_S = 3$ ft/sec, $\theta = 3^\circ$.

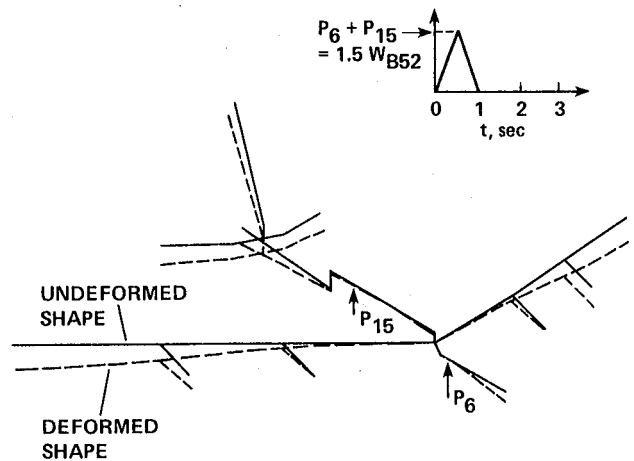


Fig. 8 Transient dynamic response of B-52 to upward triangular pulse (1.5 g) at front and rear landing gears: $t = 1$ sec, single-point constraint at grid points 12 and 13.

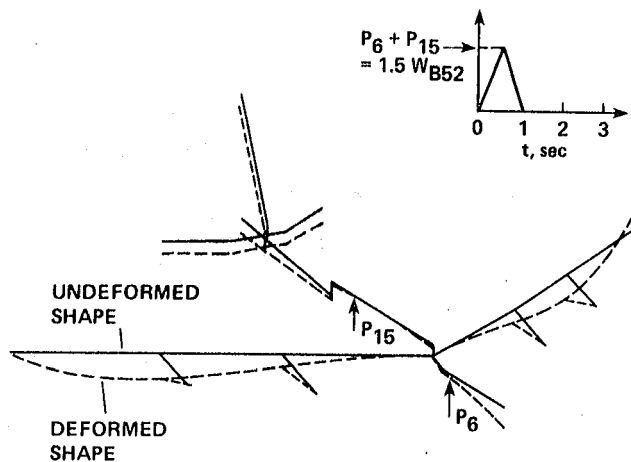


Fig. 9 Transient dynamic response of B-52 to upward triangular pulse (1.5 g) at front and rear landing gears: $t = 2.1$ sec, single-point constraint at grid points 12 and 13.

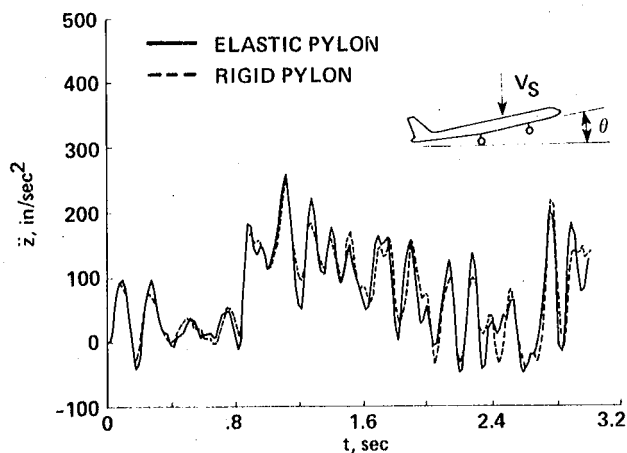


Fig. 10 z -acceleration at grid point 85 (DTV): landing, $V_S = 3$ ft/sec, $\theta = 3^\circ$.

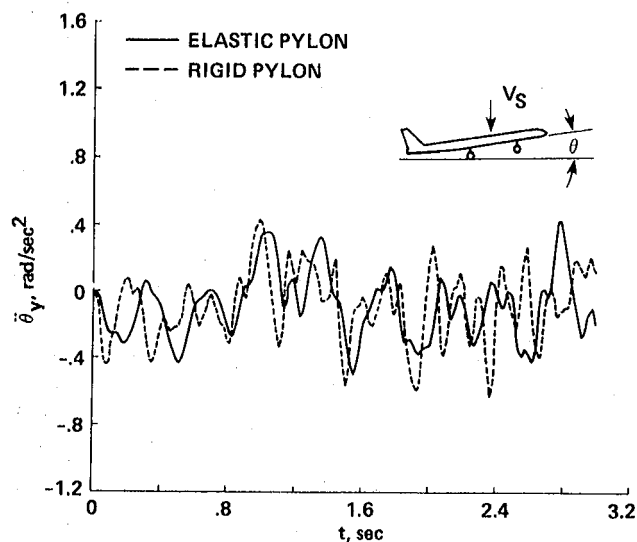


Fig. 11 Angular acceleration about y -axis at grid point 85 (DTV): landing, $V_S = 3$ ft/sec, $\theta = 3^\circ$.

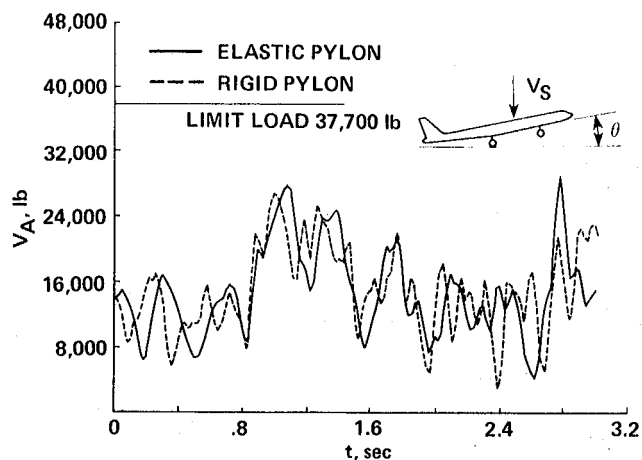


Fig. 12 Front-hook vertical load versus time: landing, $V_S = 3$ ft/sec, $\theta = 3^\circ$.

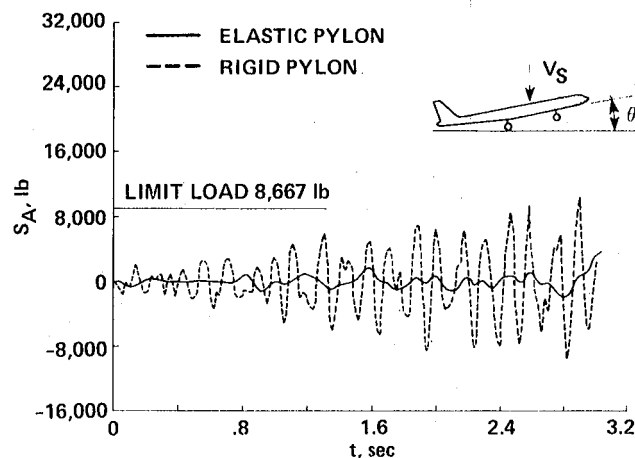


Fig. 13 Front-hook side load versus time: landing, $V_S = 3$ ft/sec, $\theta = 3^\circ$.

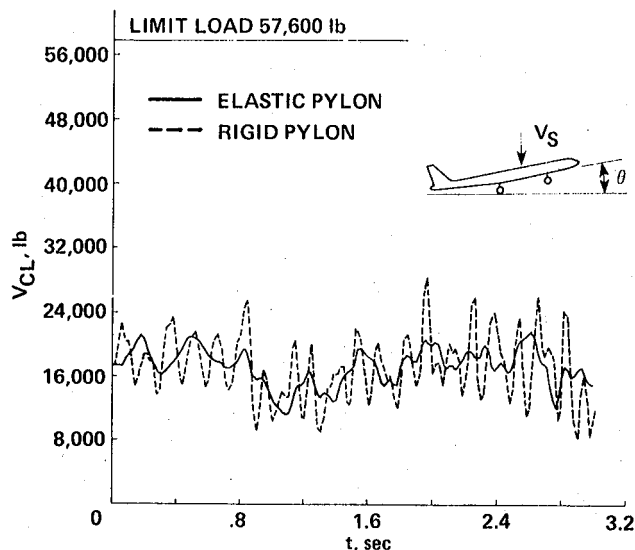


Fig. 14 Rear-hook vertical load versus time: landing, $V_S = 3$ ft/sec, $\theta = 3^\circ$.

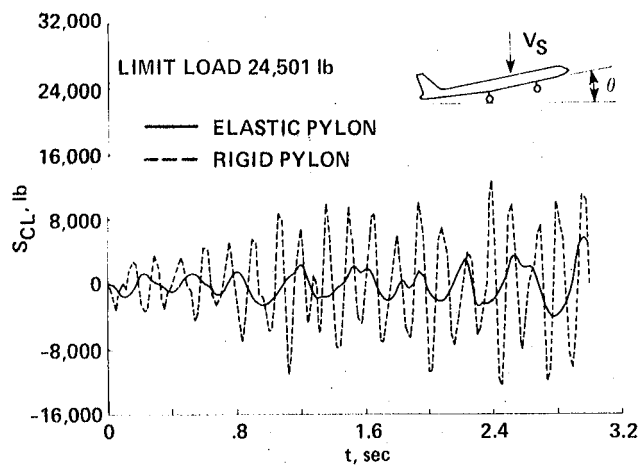


Fig. 15 Rear-hook side load versus time: landing, $V_S = 3$ ft/sec, $\theta = 3^\circ$.

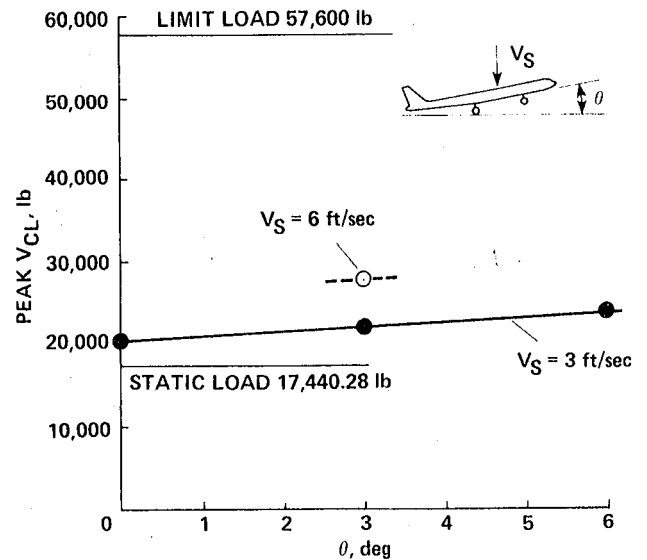


Fig. 18 Variation of rear hook peak vertical load with landing conditions.

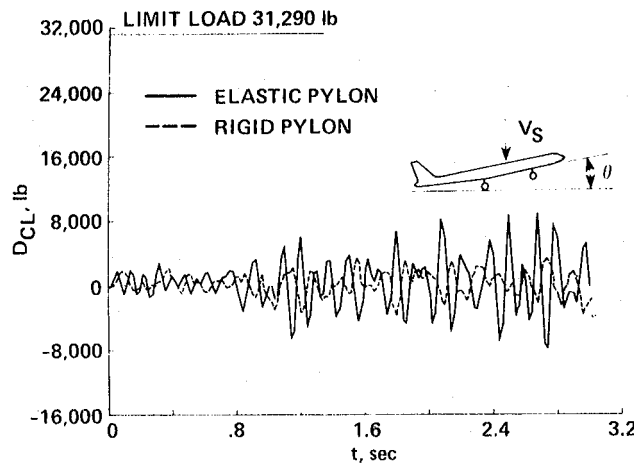


Fig. 16 Rear-hook drag load versus time: landing, $V_S = 3$ ft/sec, $\theta = 3^\circ$.

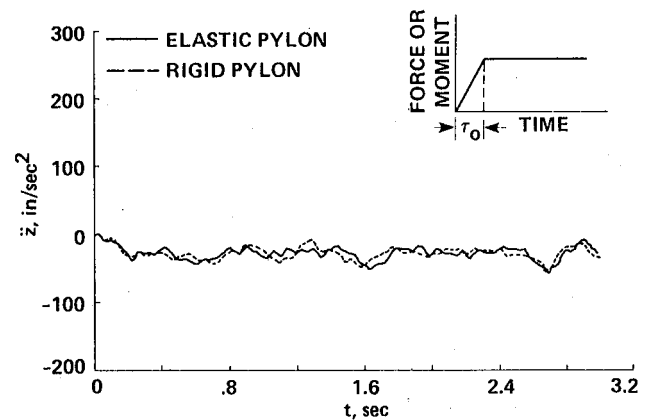


Fig. 19 z -acceleration at grid point 85 (DTV): braking, $\tau_0 = 0.2$ sec, $\mu = 0.55$.

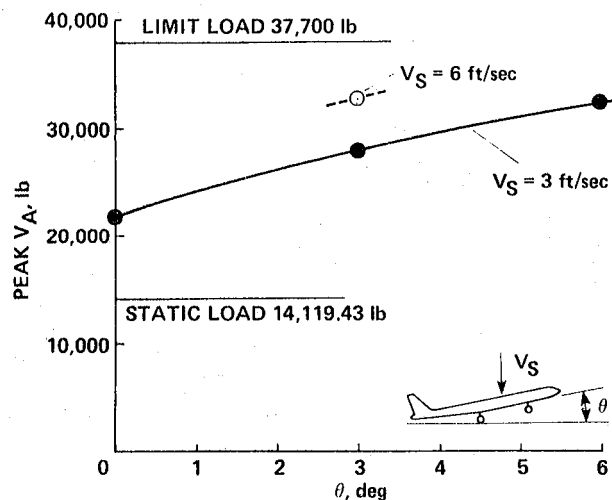


Fig. 17 Variation of front-hook peak vertical load with landing conditions.

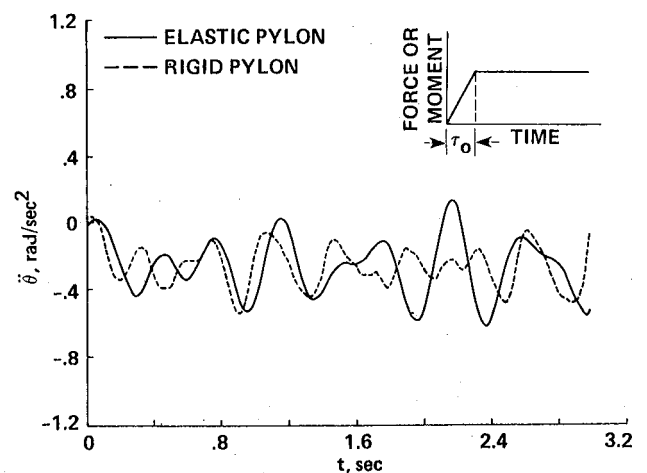


Fig. 20 Angular acceleration about y -axis at grid point 85 (DTV): braking, $\tau_0 = 0.2$ sec, $\mu = 0.55$.

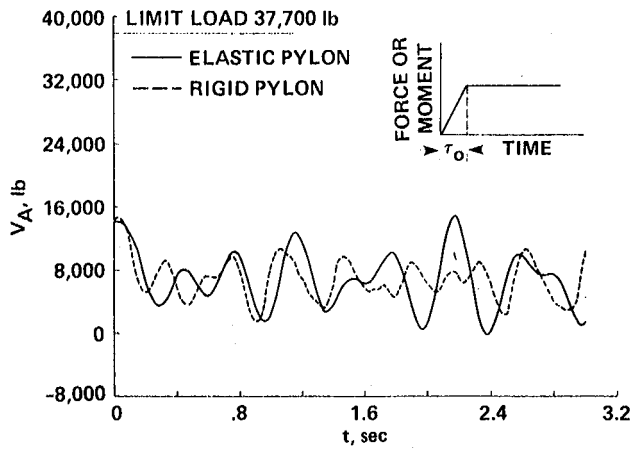


Fig. 21 Front-hook vertical load versus time: braking, $\tau = 0.2$ sec, $\mu = 0.55$.

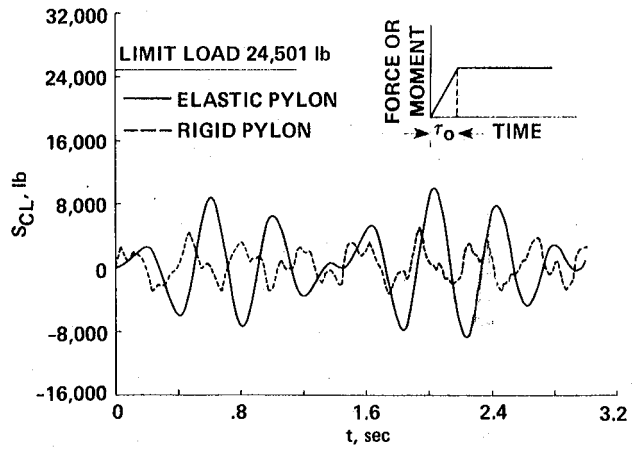


Fig. 24 Rear-hook side load versus time: braking, $\tau_0 = 0.2$ sec, $\mu = 0.55$.

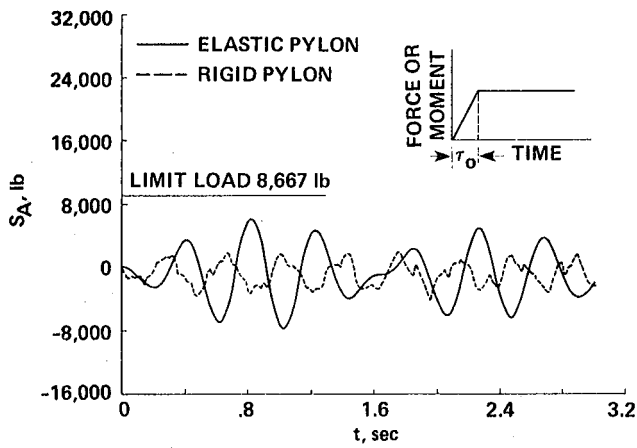


Fig. 22 Front-hook side load versus time: braking, $\tau_0 = 0.2$ sec, $\mu = 0.55$.

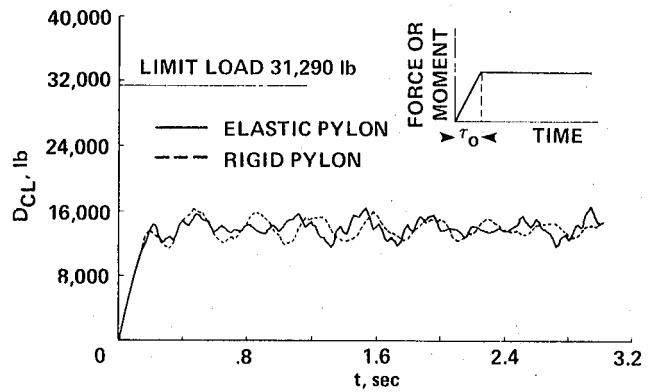


Fig. 25 Rear-hook drag load versus time: braking, $\tau_0 = 0.2$ sec, $\mu = 0.55$.

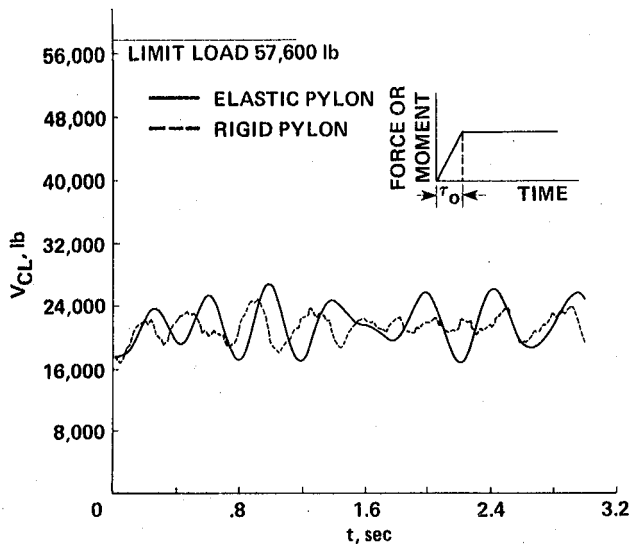


Fig. 23 Rear-hook vertical load versus time: braking, $\tau_0 = 0.2$ sec, $\mu = 0.55$.

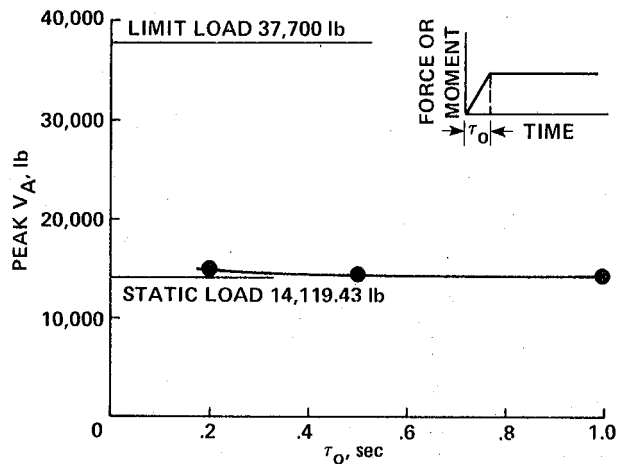


Fig. 26 Variation of front-hook peak vertical load with braking condition.

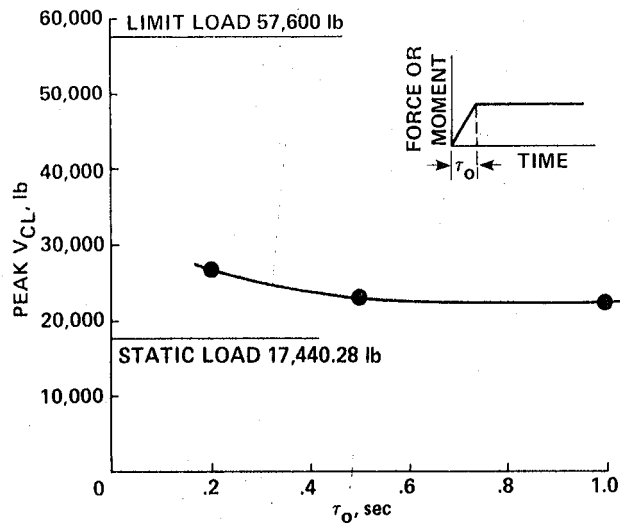


Fig. 27 Variation of rear-hook peak vertical load with braking condition.

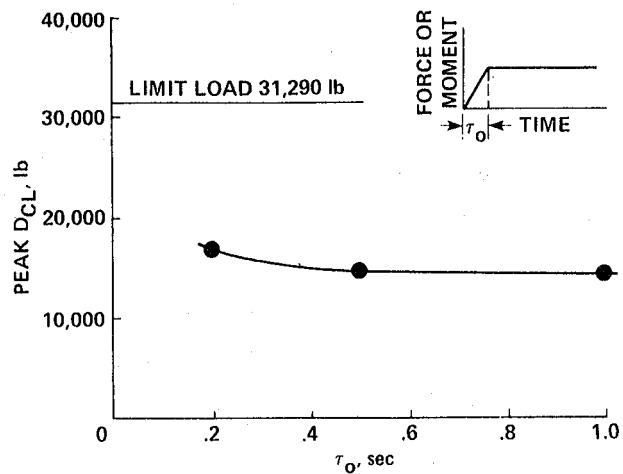


Fig. 28 Variation of rear-hook peak drag load with braking condition.

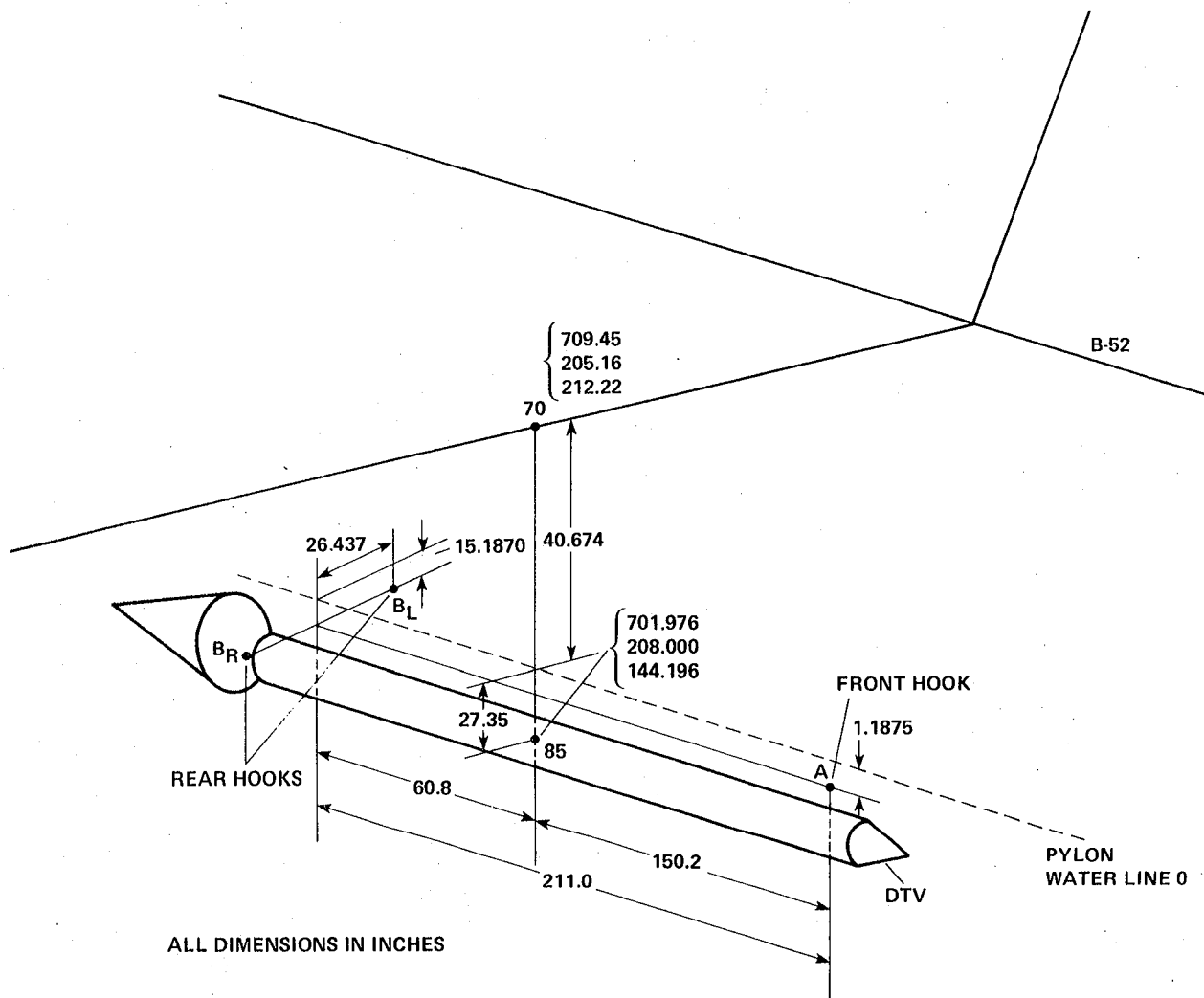
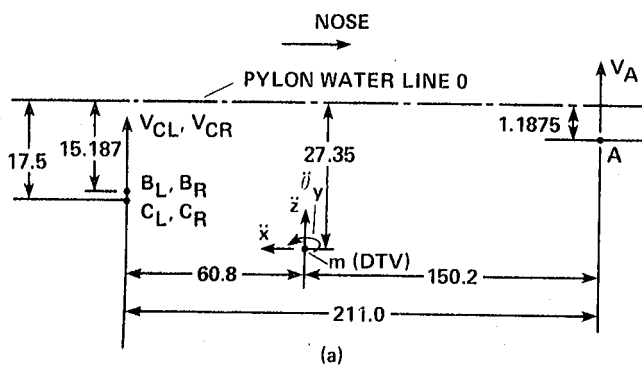
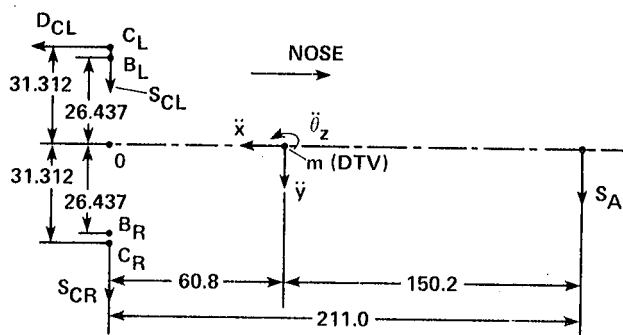


Fig. 29 Locations of DTV and front and rear hooks: Eq. (A1).



(a)



(b)

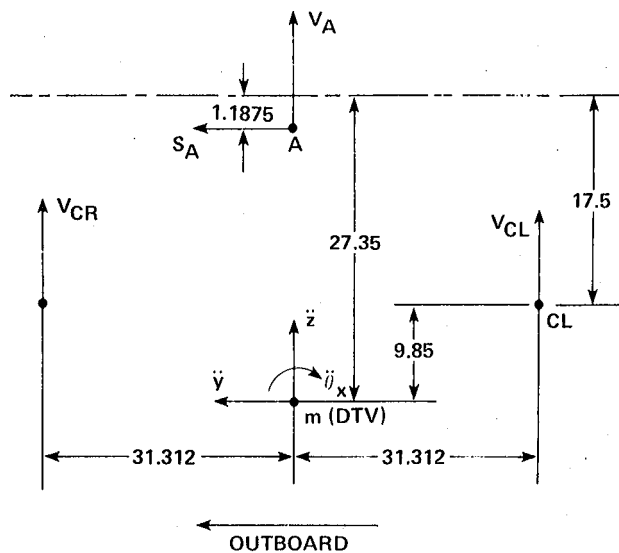
V: VERTICAL LOAD

S: SIDE LOAD

D: DRAG LOAD

ALL DIMENSIONS IN INCHES

Fig. 30 Locations of DTV and front and rear hooks: Eqs. (A4) and (A9). a) Side view; b) Top view.



FRONT VIEW

ALL DIMENSIONS IN INCHES

Fig. 31 Locations of DTV and front and rear hooks: Eq. (A5).

